International Journal of Mass Spectrometry 298 (2010) 99–110

Contents lists available at ScienceDirect

International Journal of Mass Spectrometry

journal homepage: www.elsevier.com/locate/ijms

Utilising ion mobility-mass spectrometry to interrogate macromolecules: Factor H complement control protein modules 10–15 and 19–20 and the DNA-binding core domain of tumour suppressor p53

Peter A. Faull[a,1], Hannah V. Florance[b,1], Christoph Q. Schmidt[a], Nick Tomczyk[c], Paul N. Barlow[a], Ted R. Hupp[b], Penka V. Nikolova[d], Perdita E. Barran[a,*]

[a] School of Chemistry, University of Edinburgh, West Mains Road, Edinburgh EH9 3JJ, United Kingdom
[b] Cancer Research UK p53 Signal Transduction Group, Cell Signalling Unit, Institute of Genetics & Molecular Medicine, University of Edinburgh, Edinburgh EH4 2XR, United Kingdom
[c] Waters Corporation, Atlas Park, Manchester, United Kingdom
[d] Pharmaceutical Science Division, School of Biomedical & Health Science, King's College London, Franklin-Wilkins Building, Stamford Street, London SE1 9NH, United Kingdom

ARTICLE INFO

Article history:
Received 6 March 2009
Received in revised form 8 January 2010
Accepted 11 January 2010
Available online 25 January 2010

Keywords:
Ion mobility-mass spectrometry
p53
Factor H

ABSTRACT

Ion mobility-mass spectrometry (IM-MS) has been used to study the gas-phase structures of three proteins: the DNA-binding core domain of p53 (amino acid residues 94–312) and two fragments of complement control protein factor H (regions 10–15 and 19–20) which are involved in important cellular processes. We report collision cross-sections as a function of charge state for these systems, following electrospray ionisation from 'native' conditions. The DNA-binding core domain of p53 contains a zinc ion that is postulated to have an important role in retaining functionality. We have chelated the zinc from the protein using phenanthroline and observed the conformational change in collision cross-section. Factor H region 10–15 has been interrogated and cross-sections have been elucidated for this recombinant protein that contains a number of covalently bound N-acetylglucosamine sugar molecules. Factor H region 19–20 is proposed to be an important polyanion-binding site for the intact factor H molecule (regions 1–20, 1213 amino acid residues in total) and characterising its structure by IM-MS has provided further information to the overall structure of the Factor H protein.

This work employs two different IM-MS instruments: the commercially available Waters Synapt HDMS instrument, and our Mobility Q-TOF ("MoQTOF") developed in house. Collision cross-sections obtained from identical molecular species differ to some extent between the two instruments. We observe some good agreement and some variation, with a general trend being that systems examined on the MoQTOF possess and present more compact collision cross-sections than observed with the same species on the Synapt. We attribute these differences principally to slight variations in solution conditions, effecting solution conformations and also to the differences in the source conditions and the ion transmission to the mobility devices affecting gas-phase conformations.

1. Introduction

Interdisciplinary research on the structure activity relationships of proteins has been greatly assisted by the use of mass spectrometry (MS) which can provide structural information far more rapidly than NMR or crystallography albeit somewhat 'coarse-grained'. An area of intense interest is that of whole protein mass spectrometry which relies on the transfer of an intact protein system, frequently containing multiple components, from solution phase into the gas phase [1]. This research endeavour relies on careful use of nano-electrospray ionisation (nano-ESI) to preserve non-covalent interactions from solution into the solvent-free environment of the mass spectrometer. Several experimental variables must be optimised for this to occur [2–5]: samples need to be of an adequate concentration (1 nM to 100 μM) so as to avoid unwanted aggregation, but concentrated enough to overcome mass spectrometer sensitivity and ion loss issues; samples should be sprayed from a buffer solvent that stabilises non-covalent interactions with minimal salt content; the pressure in the transfer region from atmosphere should be variable, elevated source pressures ($\sim 1 \times 10^{-1}$ mbar) above those used in traditional mass spectrometry ($\sim 1–5 \times 10^{-2}$ mbar) have been shown to assist in efficient transfer of large macromolecular species

* Corresponding author. Tel.: +44 131 650 7533.
E-mail address: perdita.barran@ed.ac.uk (P.E. Barran).
[1] These authors have contributed equally to the experimental work herein.

1387-3806/$ – see front matter © 2010 Elsevier B.V. All rights reserved.
doi:10.1016/j.ijms.2010.01.007

for MS detection due to collisional cooling. Understanding the above factors has allowed large macromolecular assemblies in excess of 1 MDa to be analysed intact [6], and has positioned mass spectrometry prominently as a tool for characterising protein structure.

Careful use of nano-ESI to retain non-covalent interactions generally produces narrow charge state distributions which can be 'read' to infer information from the mass-to-charge (m/z) ratios and their abundance on the stable forms of the protein, perhaps as a function of solvent composition, ligand concentration or pH. These methods are elegant and powerful, but only provide an indirect report on the actual conformation(s) adopted by the protein or its complex in the gas phase. The technique of ion mobility-mass spectrometry (IM-MS), which provides the collision cross-section of a given ion along with mass-to-charge information, directly reports on the molecular species shape and so provides an extra dimension to gas-phase analysis of biomolecules. Several groups have published research on whole protein IM-MS over the past decade [7–11]. Early studies by Jarrold and Clemmer studied proteins such as ubiquitin [12] (~8.5 kDa) and cytochrome *c* [13] (~12.4 kDa) to characterise collision cross-sections under a variety of physical conditions such as temperature, pH and solvent conditions. More recent efforts have achieved greater sample throughput of biomolecule mixtures [14], resolving power [15] or sensitivity [16], allowing lower abundance species to be investigated. Instrument development has been integral to these achievements. The work of Robinson et al. on the 56 kDa complex of tetrameric transthyretin used IM-MS to examine the activated form of the macromolecular complex [17]. They produced and characterised a number of gas-phase structures including tetramer and octamer species as well as a larger range of oligomeric species. This work demonstrated that activated protein assemblies can populate folded intermediate states, as measured by IM-MS, which are stable on a timescale of milliseconds prior to dissociation. A number of investigations have been focused upon the stability of protein ions in the gas phase when trapped for an extended period of time. Clemmer and co-workers [18] probed the unfolding/folding pathways of cytochrome *c* using a Paul trap and observed that ions unfold from a compact solution-phase structure when transferred to the gas phase in a relatively short time period (30–60 ms). These extended (unfolded) conformation ions are then able to adopt a number of refolded structures when trapped for extended periods (250 ms to 10 s), providing evidence for gas-phase ions to sample and adopt a number of other available structures of comparable energy. Recently Scarff et al. [9] utilised IM-MS to produce collision cross-sections of standard proteins (cytochrome *c*, myoglobin, lysozyme) in the gas phase and then compared these to published condensed-phase nuclear magnetic resonance (NMR) and X-ray crystallography (XRC) structures by computational methods using MOBCAL [19,20]. Results showed that for low charge states of proteins indicative of native structure, collision cross-sections obtained by IM-MS were in good agreement with those calculated from NMR and XRC structures. The ability to compare IM-MS data to published solution- or condensed-phase protein structures is hugely beneficial as it allows for interpretations of possible protein folding/unfolding mechanisms to be addressed as well as clarifying possible structures that are adopted in a solvent-free environment [21].

Since 2006, Synapt High Definition Mass Spectrometry (HDMS) instruments (Waters, Manchester, UK) have been utilised by research groups to elucidate and investigate protein structure in the gas phase, widening the reach of IM-MS. This instrument allows the collision cross-section (Ω) of biomolecules to be obtained through use of travelling wave ion guide (TWIG) technology [22]. Three travelling wave-enabled stacked ion ring guides are employed to trap, perform ion mobility separation on a packet of injected ions, and to transfer mobility separated ions into a time-of-flight (ToF) mass analyser. Within the separator region, a low pressure (up to 1 mbar) of nitrogen gas assists, along with a radio frequency (RF) voltage, to confine ions. A transient direct current (DC) voltage is superimposed on the applied RF of adjacent electrodes which then moves sequentially through the separator region creating a "travelling wave" sequence that propels ions through it. Ions of low mobility have a greater propensity to slip into the travelling wave behind the one in which they began than ions of higher mobility, and the ion packet is separated [23]. This experimental set up does not produce ion drift times (t_d) that are inversely proportional to ion mobility (K), therefore collision cross-section data from known reference compounds are required to provide a calibration.

Prior to the provision of the Synapt, most IM-MS measurements were conducted on home built apparatus [8,24–26] which contain drift tubes filled with an inert buffer gas though which ions travel under the influence of a static electric field. The mobility of a given ion (K) is the constant of proportionality between the drift velocity (v_d) and the electric field imposed across the drift cell (E). In these instruments, direct measurement of the rotationally averaged collision cross-section of a given ion is possible due to the relationship between drift velocity, mobility and cross-section [27]. This study contains data obtained on an instrument where collision cross-sections are determined in this way [28]. We have used this instrument successfully to obtain collision cross-sections for model protein systems and for β-defensins [28] as well as for larger macromolecular assemblies (cytochrome *c* multimers and intact haemoglobin tetramers) in excess of 60 kDa [29]. Here it is applied to the study of three protein systems which have not yet been characterised by IM-MS.

1.1. p53

As one of the most intensively studied tumour suppressors of the past two decades [30], p53 continues to provide encouraging evidence in the fight against cancer. Nicknamed the "Guardian of the Genome" [31], p53 suppresses tumour formation by inducing cell-cycle arrest, apoptosis and senescence upon cellular stress, thereby destroying DNA-damaged cells before they can proliferate [32]. As a highly sequence specific DNA-binding transcription factor, p53 concentration is maintained at low resting levels due to interactions with the E3 protein ligase MDM2 (mouse double minute 2) [33,34]. MDM2 maintains p53 concentration at low levels *via* an autoinhibitory feedback loop which mediates ubiquination and degradation of p53 [35]. Interaction between MDM2 and p53 has been shown to occur at the N-terminal domains of both molecules [36] with three buried amino acid residues of p53 binding in a deep hydrophobic binding cleft on MDM2 [32]. p53 binds to DNA through a structurally complex domain which is stabilised by a tetrahedral geometry zinc ion bound by three cysteine and one histidine residues [37]. This metal atom plays a regulatory role in the control of p53 folding and DNA-binding activity. Meplan et al. [38] have investigated the role of metal binding on the stability of the p53:DNA complex, revealing zinc chelation disrupts the architecture of the p53-binding domain which results in rapid cysteine oxidation and disulphide-linked aggregate formation. Meplan prepared a recombinant form of p53 lacking zinc. Upon addition of zinc at physiological concentrations (~5 μM), renaturation and reactivation of p53 occurred, allowing DNA-binding to occur. They further investigated this with a range of divalent metals and found that Co^{2+} at concentrations of ~125 μM had a similar effect, implying that the metal atom acts to hold the domain in a favourable conformation for DNA-binding to occur.

p53 (~43.7 kDa) is composed of 393 amino acids and is divided into three major regions: a central DNA-binding core domain, the C-terminal tetramerisation domain and the N-terminal transacti-

vation domain [39,40]. The core domain has been characterised by NMR spectroscopy [41] (*vide infra*) and it is in this region that p53 inactivation mutations have been shown to occur in up to 50% of human cancers. [42] Further studies of the structure of the p53 core domain and its interaction with DNA may provide possibilities for new drug discoveries, which could be exploited in cancer therapies.

1.2. Factor H

Factor H (fH) is a large complement control protein which circulates in plasma and directs the immune system to act on pathogens rather than damaging host tissue. The main role of this soluble glycoprotein is to regulate the Alternative Pathway of the complement system, a biochemical cascade that removes pathogens from an organism, and can operate without antibody participation [43,44]. fH (155 kDa, 1213 amino acid residues) is composed of twenty complement control protein modules joined in a "string-of-beads" arrangement by nineteen short, potentially flexible, linking sequences of three to eight residues [45]. Variations in polyanion-binding sites within the protein are connected to a number of complement-mediated diseases including atypical haemolytic uremic syndrome [46] and age-related macular degeneration [47]. Mapping of these polyanion sites have been rigorously investigated by Schmidt et al. [45].

In this work, two covalently bound regions of complement control protein modules have been studied: modules 10–15 and modules 19–20 (C-terminal domain) denoted fH 10–15 and fH 19–20 respectively. The solution structure for fH 19–20 has been determined by NMR experiments [48] and the binding sites and affinity of glycosaminoglycans (GAGs), sulfated heparin-derived tetrasaccharides, have also been investigated for many of the complement control protein regions, including fH 10–15 and fH 19–20 [45]. Understanding the structure of the protein and the conformation(s) it adopts to bind GAGs and C3b (a cleavage product of complement component 3) are fundamental to learning more of the mechanisms Factor H employs in its regulatory role. Ion mobility combined with mass spectrometry, with a much higher upper size limit than NMR is here used to provide a good platform for initial investigations of the structure and dynamics of interaction of the modules of this important biological system.

2. Experimental

2.1. Synapt HDMS Instrument

p53 DNA-binding core domain data were acquired on a Synapt HDMS instrument (Waters, Manchester, UK) in positive ionisation mode. All samples were sprayed *via* a Nanomate (Advion Biosciences, Ithaca, NY) with the capillary voltage set between 0.5 and 1.5 kV adjusted to maintain stable spray. Source pressure was optimised for signal transmission. Acquisition parameters were obtained to provide optimal ion mobility separation: cone voltage 40 V, trap region collision energy 5 eV, and source temperature 120 °C. Within the ion mobility separator region of the Synapt, nitrogen gas was present at a pressure of 0.51 mbar. Velocity and wave height of the travelling wave were varied to obtain optimal signal. Discrete wave heights of 6, 8 and 10 V as well as a wave height gradient of 8–10 V were employed. For all collision cross-section measurements a discrete wave height of 8 V was employed for samples and calibrant acquisition. Equine heart cytochrome *c* and equine myoglobin were purchased from Sigma–Aldrich (St. Louis, MO, USA), with 0.2 mg mL^{-1} dissolved in 50/50 by volume water/acetonitrile containing 0.1% formic acid were examined under identical conditions as those used for each protein system to produce calibration curves so as to obtain collision cross-sections from the mobility measurements according to the methods outlined by others [49]. Arrival times for ions from the calibrant species, bracket those for the ions of the proteins under study (see supplementary data) thus minimising the chance of calibration errors.

2.2. MoQTOF Instrument

Mass spectra were acquired on a modified Q-ToF 1 (Waters, Manchester, UK) quadrupole time-of-flight mass spectrometer possessing a 5.1 cm copper drift cell for mobility measurements [28]. Ions were produced by positive nano-electrospray ionisation using a Z-spray source, within a spray voltage range of 1.85–2.10 kV and a source temperature of 80 °C. Sample and extractor cone voltages were optimised to maintain a stable signal, source pressures were also optimised for each system. Nanospray tips were prepared in-house from borosilicate glass capillaries (Kwik-Fil, World Precision Instruments Inc., Sarasota, FL, USA) using a Flaming/Brown Micropipette puller (Model P-97, Sutter Instrument Co., Novato, USA). Tips were filled with 10–15 μL of sample using gel loader tips (Eppendorf, Hamburg, Germany). Ion mobility experiments were performed at ~3.2 Torr helium pressure and ~300 K cell temperature. The drift voltage across the cell was varied to obtain ion mobility data by decreasing the cell body potential from 60 to 15 V. All mobility data was obtained from plots of arrival time versus drift voltage over this range. Measurements were taken at six or more distinct voltages. A minimum of 2000 scans were collected for each drift voltage. Data was analysed using modified MassLynx v4.1 software (Waters, Manchester, UK) and processed using Microsoft Excel and Origin 7.5 (Origin Lab) to determine collision cross-sections from arrival times over a range of drift voltages. Arrival time distributions containing more than one conformer (evidenced by shoulder or wide peaks) were fitted using a non-linear fitting tool in Origin. Two or more Gaussian curves of shared width were fitted to the data and iterations were performed until convergence. Midpoints (scan number) of both curves were obtained and converted to arrival time by multiplying by the pusher period. These were then plotted as a function of drift cell pressure divided by drift voltage (P/V) to obtain the slope of the linear fit. Only linear fits with a R^2 value greater than 0.9990 were accepted. The gradient of the accepted linear fits were then converted to collision cross-sections (Ω) as detailed elsewhere [28,29].

2.3. p53 protein

Cloning of wild-type human p53 (amino acid residues 94–312; M_R = 24,615.5 Da in the presence of a zinc ion) was performed using pRSETA expression vector (Invitrogen) which was modified so that it did not contain the His tag [50]. Protein was expressed at 37 °C in *Escherichia coli* C41 cells (Avidis) and grown up to an O.D. of 0.8. The temperature was reduced to 22 °C before cell cultures were induced with 1 mM IPTG and grown overnight. Cells were harvested at 4 °C and lysed using Bug Buster Protein Extraction Reagent (Novagen). Benzonase nuclease (Novagen) and EDTA-free protease inhibitor tablets (Roche) were also used during this process. The soluble fraction was loaded onto an SP Sepharose column (GE Healthcare), eluted with a NaCl gradient followed by gel filtration chromatography using HP26/60 Superdex 200 column (GE Healthcare) [51,52]. Protein samples were snap-frozen in liquid nitrogen and stored in 25 μL aliquots at −80 °C. One hour before use, an aliquot was thawed and dialysed in 20 mM ammonium acetate. 10% by volume propan-2-ol was added prior to analysis by mass spectrometry if required to give a final protein concentration of 20 μM. For zinc chelation, 1 mM aqueous phenanthroline was added prior to dialysis.

2.4. Factor H 10–15 protein

DNA sequences encoding fH 10–15 (residues 568–927 numbered on the basis of encoded protein sequence, *i.e.*, before removal of secretion signal; M_R = 40,909.4 Da) were cloned into the *Pichia pastoris* expression vector pPICZα (Invitrogen). Expressed proteins were directed to the secretory pathway by placing the coding sequence behind the *Saccharomyces cerevisiae* α-mating factor secretion sequence. Following transformation into *P. pastoris* strain KM71H (Invitrogen), proteins were expressed in shaker flasks or a fermentor. Anion-exchange chromatography was used as a first purification step and was followed by gel-filtration chromatography. N-linked glycosylation was deglycosylated before purification by incubating 100 mL supernatant with 6000 U EndoHf (New England Biolabs) at 37 °C for 3 h. Yields were typically 0.1–0.5 mg of pure protein per gram of wet cells. Samples were dialysed into 20 mM ammonium acetate using a Mini Dialysis Kit with a 1 kDa cut-off (Amersham Biosciences Corp., NJ, USA) to a final stock concentration of ~200 μM. For mass spectrometry analysis, stock was diluted to 25 μM in 20 mM ammonium acetate and 10% by volume propan-2-ol was added. An additional two amino acids, alanine and glutamic acid, are present on the sequence due to a recombinant impurity, adding a mass of 200.2 Da.

2.5. Factor H 19–20 protein

The fragment containing human fH 19–20 (residues 1107–1231 native sequence numbering; M_R = 14,743.8 Da) was cloned into the *P. pastoris* expression vector pPICZα. Expressed fH 19–20 was directed to the secretory pathway by placing the coding sequence behind the *S. cerevisiae* α-mating factor secretion sequence. Inefficient cleavage of this secretion signal combined with cloning artefacts resulted in the additional sequence EAEF at the N terminus. Cation-exchange chromatography was used to purify fH 19–20 collected from the culture supernatant. Samples were dialysed into 20 mM ammonium acetate using a Mini Dialysis Kit with a 1 kDa cut-off (Amersham Biosciences Corp., NJ, USA) to a final concentration of ~500 μM. For mass spectrometry analysis, stock was diluted to 75 μM in 20 mM ammonium acetate and 10% by volume propan-2-ol was added. An additional two amino acids, alanine and glutamic acid, are present on the sequence due to a recombinant impurity, adding a mass of 200.2 Da.

3. Results and discussion

3.1. p53 containing zinc mass spectrometry

Fig. 1 presents two mass spectra, one obtained on a Synapt HDMS instrument and the other on the MoQTOF, for p53 sprayed from buffered solutions containing 10% by volume propan-2-ol. Both mass spectra have the same dominant peaks $[M+zH+Zn]^{z+}$ assigned to the $z = 9^+$ and 10^+ charge states, of p53 containing a zinc ion (calculated M_R = 24,615.5 Da, observed Synapt M_R = 24,613.2 Da and MoQTOF M_R = 24617.2 Da). These two peaks indicate the protein is in a well folded structural state as there are a limited number of charge accessible residues available for protonation. Two dimeric species, $[2M+zH+Zn]^{z+}$ z = 13 and 15, are observable and formed in solution, representing higher order multimeric association. Low abundance peaks (<20% ion intensity) are present for a number of higher charged species, $16 \leq z^+ \leq 11$ indicative of a small amount of protein unfolding.

3.1.1. Comparison

Mass spectra for native p53 differ somewhat between the Synapt and the MoQTOF. Charge state distributions are similar, with the base peak varying by a single charge state (9^+ in Synapt, 10^+ in MoQTOF). MoQTOF charge state intensity decreases at higher charge, whereas signal decreases to charge state 13^+ and increases again to a maximum at 16^+ in Synapt data, indicating the presence of more denatured protein molecules, and suggesting that the source conditions are not quite optimised for native protein nano-ESI. Multimeric species signal intensity (dimer) is more pronounced in the MoQTOF data.

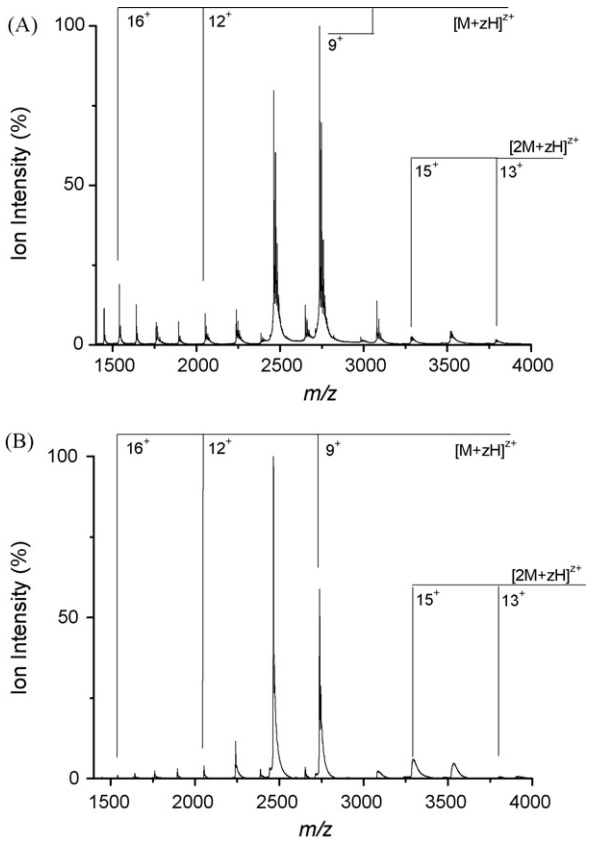

Fig. 1. Mass spectra collected on a Synapt HDMS instrument (A) and collected on the MoQToF instrument (B) of native-like p53 sprayed from 20 mM ammonium acetate showing monomer and dimer peaks (+10% propan-2-ol for Synapt spectrum).

Fig. 2 is a Synapt "Heatmap" which plots m/z against drift time (bin number) for native p53 at an experimental wave height of 8 V. Charge state increases from the top to the bottom of the plot, with ions of the same m/z value (y ordinate) but different drift time (x ordinate) clearly displayed. This plot provides initial information regarding the extent of unfolding of a particular charge state, as

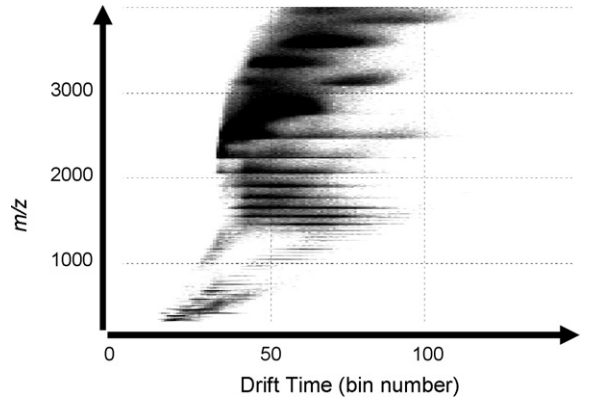

Fig. 2. Synapt HDMS "Heatmap" plot of m/z versus drift time (bins) for native p53.

the presence of more extended (open) conformers will increase the length of the *x* ordinate line at a single *m/z* value.

3.2. p53 with zinc removed mass spectrometry

3.2.1. Synapt

p53 with zinc removed was analysed using the Synapt (observed M_R = 24,550.2 Da; mass spectrum in supplementary data) and displays a wider charge state distribution than that of zinc-bound p53. Charge states ranged from $z = 9^+$ to 16^+ in the experimental range acquired (1500–3000 *m/z*) with $z = 10^+$ the most dominant peak. The wider charge state distribution can be attributed to loss of tertiary structure, possibly in the zinc-binding domain, and facile protonation of solvent exposed basic residues.

3.2.2. MoQTOF

Mass spectra of p53 with zinc removed (MoQTOF observed M_R = 24,550.8 Da; mass spectrum in supplementary data) analysed on the MoQTOF displays a charge state distribution of peaks from $z = 7^+$ to 12^+ which again is wider than that obtained prior to chelation. Charge states $z = 7^+$ to 10^+ have a second peak at higher *m/z* value that can be assigned to p53 containing zinc, indicating full chelation of the metal was not achieved because an insufficient concentration of phenanthroline was added or the incubation period was not long enough (however both parameters were the same in Synapt and MoQTOF experiments). At charge states greater than 10^+, this peak is not observed indicating the protein can no longer stabilise the metal ion. The dominant low charge state of $z = 10^+$ suggests that p53 has not denatured extensively in the absence of zinc. Dimer peaks of attributable to $[2M+15H]^{15+}$ (3274.3 *m/z*) and $[2M+13H]^{13+}$ (3777.9 *m/z*) were also observed.

3.2.3. Comparison

MoQTOF displays a more "native-like" mass spectrum than Synapt when the protein has been subjected to zinc removal using phenanthroline. One would expect that removing a binding site stabilising entity (the zinc ion) would promote formation of a less structured arrangement, as displayed by the Synapt data. However, MoQTOF data shows that within the gas phase, removal of the zinc has had a less detrimental effect on the overall structure under these solvent conditions. This is supported by the experimental work by Meplan et al. [38] (as detailed in the introduction) as removal of zinc produces physiologically inactive p53, whereas addition renatures the protein. This suggests that the overall structure is not altered (denatured) to such an extent that the zinc-binding region cannot be easily restored. This is shown in the MoQTOF data and suggests a gentler desolvation of proteins before ion mobility interrogation relative to Synapt analysis with the source conditions we used. An alternative explanation is that the less than full chelation of zinc for the solution sprayed on the MoQTof is responsible for the more native like protein mass spectrum observed.

3.3. p53 containing zinc ion mobility-mass spectrometry

3.3.1. Synapt

A wide charge state range for $[M+zH]^{z+}$ $z = 7^+$ to 17^+ was obtained for p53 containing zinc, of good enough intensity for a total of fifteen collision cross-sections to be determined at a wave height of 8 V. These are plotted as a function of charge state (closed squares) in Fig. 3A, with collision cross-section data in Table 1. Cross-section is observed to increase with increasing charge (*z*) and is attributed to protein unfolding upon protonation. Protonation sites are likely to be basic residues as there are 19 arginine, 8 lysine and 9 histidine residues available in the p53 molecule. Unfolding occurs to overcome Coulombic repulsion. The lowest two charge states, $z = 9^+$

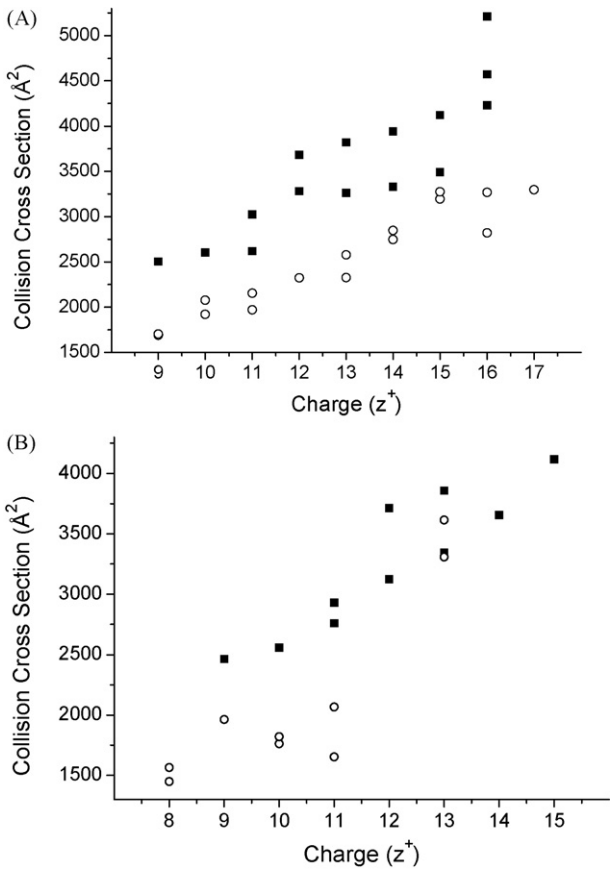

Fig. 3. Collision cross-sections versus charge (*z*) obtained on the Synapt (closed squares) and MoQTOF (open circles) for p53 containing zinc $[M+Zn+nH]^{z+}$ (A). Collision cross-sections versus *z* obtained on the Synapt (closed squares) and MoQTOF (open circles) for p53 with zinc chelated $[M+zH]^{z+}$ out as described in the text (B). Data on the MoQTOF for $z = 12$ was not of good enough quality to include for reasons described in the text.

Table 1
Collision cross-sections of native p53 (containing zinc) obtained from Synapt and MoQTOF data.

Charge state (z^+)	Collision cross-section (Å²) on Synapt	Collision cross-section (Å²) on MoQTOF
9	2503	1689 1703
10	2604	1920 2076
11	2619 3026	1969 2154
12	3282 3682	2324 –
13	3263 3822	2327 2577
14	3331 3941	2748 2848
15	3491 4121	3195 3276
16	4231 4572 5211	2820 3269 –
17	–	3298

and 10^+ provide single resolvable conformers (with collision cross-sections of 2503 and 2604 Å^2 respectively). At these low charge states the protein is believed to be in native-like, compact conformations. With increasing charge ($z = 11^+$ to 15^+) two conformers can be elucidated which indicates that multiple gas-phase structures are produced, since these have larger collision cross-sections than those seen for the lower charge states these conformations must be indicative of unfolding states of the protein. At a higher charge, $z = 16^+$, the observed collision cross-section continues to increase and up to three resolvable gas-phase conformations are produced (4231, 4572 and 5211 Å^2). Although p53 has unfolded to a more extended structure it is still retaining some non-covalent interactions (presumably through hydrogen bonds and electrostatic interactions) that sustain the protein in these three distinguishable conformations for the duration of the mobility experiment.

3.3.2. MoQTOF

A slightly wider charge state range was obtained on the MoQTOF ($z = 9^+$ to 17^+) when p53 was sprayed from 20 mM ammonium acetate buffer. Unlike Synapt analysis, addition of 10% propan-2-ol was not required to obtain a good strong signal and in fact when added, was detrimental to signal strength (data not shown) which suggests a difference in the desolvation of each source. Collision cross-sections for p53 are smaller for all charge states when compared with Synapt data, with cross-sections ranging from 1689 Å^2 for $z = 9^+$ to 3298 Å^2 for $z = 17^+$. For seven of the nine charge states, two conformations were elucidated (only one resolvable conformation for $z = 12^+$ and 17^+). These are plotted as a function of charge state (open circles) in Fig. 3A, with collision cross-section data in Table 1, alongside Synapt data. Low charge states adopt compact conformations, with unfolding occurring as z is increased. The two conformations observed for both $z = 14^+$ and 15^+ differ by only 3.5% and 2.5% respectively, indicating similar gas-phase structures may be adopted at this charge state.

Dimer signal intensity in both instruments was insufficient to calculate cross-sections. Potentially, dimer molecules of p53 may be dissociating in the gas phase and contribute to the monomeric species abundance.

Compact conformations are observed from both data sets at low charge states, and increase with increasing charge. MoQTOF values are >8.5% smaller than Synapt values for native p53 with respect to charge ($z = 15^+$, 3195 Å^2 MoQTOF versus 3491 Å^2 Synapt). We have attributed this predominantly to greater source pressure control in the MoQTOF, allowing gentler desolvation to occur and a more compact gas-phase structure compared with Synapt sampling which give rise to partially unfolded proteins. The variation in cross-section between data taken on each instrument highlights the need to take care with source conditions when performing native ESI experiments. To check the MoQTOF p53 values, we spiked a solution with cytochrome *c*, which yielded the same collision cross-sections as previously reported [28] which are commonly employed for Synapt calibration [49].

3.4. p53 with zinc removed ion mobility-mass spectrometry

3.4.1. Synapt

Collision cross-sections obtained for p53 with zinc removed are in Table 2 and plotted as a function of charge state in Fig. 3B. Seven charge states were visible in the Synapt IM-MS spectrum with $z = 9^+$ to 15^+ (wave height 8 V). At the two lowest charge states, $z = 9^+$ and 10^+, single conformations were resolved with collision cross-sections of 2464 and 2558 Å^2 respectively. At these low charge states, structure is most likely of a compact native-like form but loss of the zinc atom probably causes some structural rearrangement. For $z = 11^+$ to 15^+ (excluding 14^+), two conformations for each charge state were successfully resolved. In comparison with the data obtained for p53 containing zinc, low charge states ($z = 9^+$ and 10^+) are more compact, with a smaller collision cross-section in the absence of zinc and may have undergone gas-phase collapse. Increasing charge appears to increase collision cross-section in a near linear fashion for smaller Synapt conformers again attributable to Coulombic unfolding.

Table 2
Collision cross-sections of p53 with zinc chelated out obtained from Synapt and MoQTOF data.

Charge state (z^+)	Collision cross-section (Å^2) on Synapt	Collision cross-section (Å^2) on MoQTOF
8	–	1450 1566
9	2464	1963
10	2558	1763 1820
11	2760 2931	1953 2067
12	3124 3712	–
13	3344 3856	3309 3614
14	3655 –	–
15	3542 4115	–

Cross-sections for low charge states ($z = 9^+$ to 12^+) are smaller in the absence of zinc than compared with those obtained with zinc present (native p53) by up to 4.8% (12^+ smaller conformer). This suggests that zinc allows a more ordered native geometry to the protein, stabilising it against any coulombically driven gas-phase unfolding. This trend reverses at higher charge states, with larger cross-sections in the absence of zinc above $z = 12^+$ compared with the equivalent native p53 charge state, which indicates that the bound metal ion stabilises the protein tertiary fold, and when absent the protein unfolds coulombically more readily.

3.4.2. MoQTOF

Cross-sections for five charge states ($z = 8^+$ to 11^+ and 13^+) of p53 with zinc removed are in Table 2 and plotted as a function of charge state in Fig. 3B alongside Synapt values. Data for $z = 12^+$ was very weak (see below) and has been omitted. Cross-sections are all smaller than Synapt however at charge state $z = 13^+$, the smaller conformer is only 1% smaller. At low charge states ($z = 8^+$ to 11^+), cross-sections for zinc removed p53 are smaller than those for the equivalent charge for zinc present native p53 by up to 12.3% for the larger $z = 10^+$ conformer.

The data taken on the Synapt displays a near linear increase in cross-section with charge to complement unfolding due to Coulombic repulsion. MoQTOF data is again smaller than Synapt, but shows a more sustained cross-section at low charge, with a sudden large unfolding transition from $z = 11^+$ to 13^+. The arrival time distribution for $z = 12^+$ was very broad with signal intensity spread over a large number of arrival bins, which suggests that this charge state at the unfolding transition presents a large number of conformations. The intensity of the peak in the mass spectrum is low which also suggests this is an unstable ion. With respect to the larger Synapt data, it is possible that heating due to the RF field in the T-wave device may induce larger cross-sections for higher charge species, *i.e.*, protein molecules with a higher charge will unfold more. Evidence for this can also be found in the data presented next for Factor H, in particular for the modules 10–15.

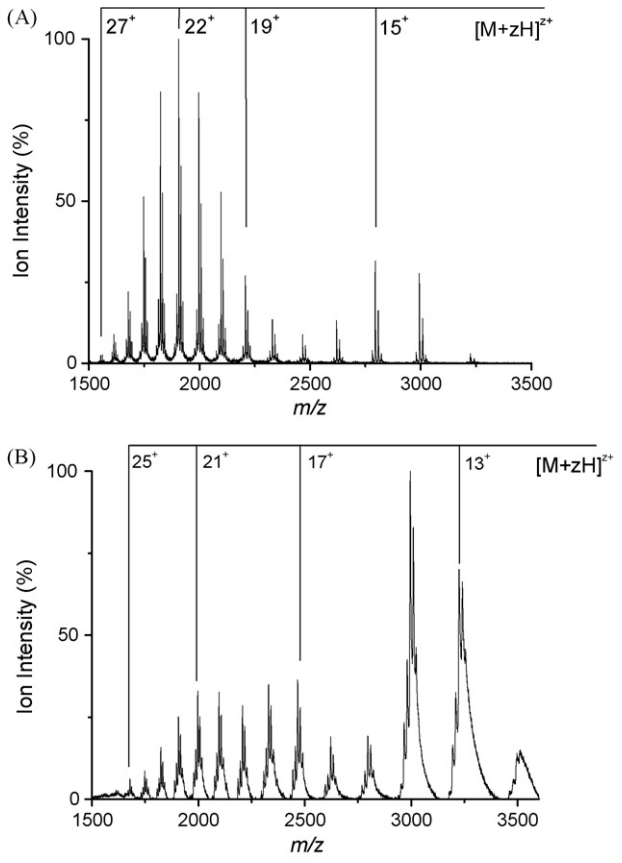

Fig. 4. Mass spectra of native-like fH 10–15 sprayed from 20 mM ammonium acetate and 10% propan-2-ol on the Synapt (A) and the MoQTOF (B).

3.5. fH 10–15 mass spectrometry

3.5.1. Synapt

fH 10–15 (M_R = 40,909.4 Da) was sprayed under native-like buffer conditions with 10% by volume propan-2-ol added to assist desolvation. Under these solvent conditions, a wide charge state range was observable in the mass spectrum (Fig. 4A) indicative of a more unfolded structure than would be expected spraying from buffer. The charge state distribution ranges from $z = 13^+$ to 27^+ with a bimodal distribution centered on $z = 15^+$ and 22^+. For each charge state, a series of peaks indicated three to six bound N-acetylglucosamine (GlcNAc) molecules (M_R = 220 Da; mass spectral peaks are separated by 203 *m/z* as loss of 17 Da occurs to covalently attach the sugar to asparagine residues). These are artefacts from the expression method and within the mass spectrum, the four sugar molecules bound peak is most abundant. Also as a consequence of the expression system, two additional amino acid residues, glutamic acid (E) and alanine (A) are present at the N-terminal and increase the protein mass by 200.2 Da.

3.5.2. MoQTOF

fH 10–15 was sprayed from the same solvent conditions as those on the Synapt and is shown in Fig. 4B. A similarly wide charge state distribution was observed but shifted to $z = 12^+$ to 26^+, and with a trimodal distribution with peaks at 14^+, 17^+ and 21^+. The relative abundance of the lower charge states indicates a more native-like protein (like that of p53 with zinc removed) supporting that the MoQTOF is able to successfully transfer relatively large (~41 kDa) molecular complexes into the gas phase. Two to five bound GlcNAc sugar molecules are observed with four bound sugars dominant (the sixth bound sugar molecule is poorly resolved, but present).

3.6. fH 10–15 ion mobility-mass spectrometry

3.6.1. Synapt

Cross-sections for four fH 10–15 species were elucidated and are presented in Table 3. Three to six bound N-acetylglucosamine (GlcNAc) sugar molecules are observed on each charge state with four bound sugars dominating. At low charge states, cross-sections for three, four and five bound sugars to the protein are either the same or within 5% of each other, indicating structural similarity. As charge increases, collision cross-section increases and a large rate of cross-section change is observed between $z = 18^+$ and $z = 22^+$ for all species indicating a loss of interactions between domains (plot not shown). This is observed most with the four sugar bound species with an increase of 1876 Å^2 from $z = 18^+$ (2615 Å^2) to $z = 22^+$ (4491 Å^2), and further charge sequestering at $z = 22^+$ to 26^+ shows a small increase in cross-section.

Table 3
Collision cross-sections (Å^2) of Factor H 10–15 with 3–6 N-acetylglucosamine molecules bound obtained from Synapt data.

Charge state (z^+)	+3 GlcNAc molecules	+4 GlcNAc molecules	+5 GlcNAc molecules	+6 GlcNAc molecules
13	–	2183	2183	–
14	2196	2196	2196	2225
15	2301	2202	2202	2236
16	2397	2323	2342	2396
17	2481	2460	2460	2519
	3032	2889	2922	2938
	3713	3713	3639	3664
18	3155	2615	2636	2718
	3941	3169	3200	3348
19	3544	3443	3494	3510
	3974	3988	4072	4030
20	3669	3841	3857	3858
	4130	4340	4310	4339
21	3861	3879	3916	4162
	4377	4425	4439	–
22	4474	4491	4457	4508
23	4519	4556	4556	4575
24	4643	4623	4623	4541
25	4629	4651	4628	4759
26	4775	4775	4751	4774

Table 4
Collision cross-sections (Å^2) of Factor H 10–15 with 2–5 N-acetylglucosamine molecules bound obtained from MoQTOF data.

Charge state (z^+)	+2 GlcNAc molecules	+3 GlcNAc molecules	+4 GlcNAc molecules	+5 GlcNAc molecules
13	2570	2597	2600	2608
14	2546	2559	2538	2577
15	2820	2761	2722	2738
16	2970	2821	2778	2793
17	3005	2972	2853	2741
18	3105	3028	2992	3132
19	3194	3387	3319	3308
20	3430	3573	3547	3827
21	3577	3660	3919	3550
22	3564	3750	4157	3945
23	3675	3895	4035	3881
24	3973	4154	4065	4122
25	–	4616	4102	4331

3.6.2. MoQTOF

IM-MS data for fH 10–15 provided a large number of cross-sections due to the presence of covalently bound GlcNAc sugar molecules. Cross-sections for two, three, four and five bound sugar molecules were acquired over a charge state range of 13^+ to 25^+ (12^+ and 26^+ ion mobility signal was too weak to obtain cross-sectional data) with the trend in increasing cross-section increasing with charge (Table 4).

At low charge states, $z = 13^+$ and 14^+, cross-sections for all four species are within two standard deviations of the mean cross-section at that charge state (13^+ average cross-section = 2594 Å^2 with $2\sigma = 33$; 14^+ average cross-section = 2555 Å^2 with $2\sigma = 34$). This implies a similar structure for all species and suggests that the covalently bound sugar molecules are folded back against the protein surface (as opposed to projecting away from the protein surface—it is assumed this would increase cross-section to a greater extent) and non-covalently interacting with available hydrogen bonds and electrostatic regions to reduce their exposed surface area. Similarities in cross-section cease as charge increases above $z = 15^+$. fH 10–15 cross-sections with two bound GlcNAc molecules had the smallest cross-sections overall, whereas four and five bound sugar molecules to fH 10–15 showed greater increase in cross-section at higher charge.

Over the entire charge state range, three bound GlcNAc showed the greatest increase in cross-section from 2597 Å^2 at $z = 13^+$ to 4616 Å^2 at $z = 25^+$ ($\Delta = 2019$ Å^2). These observations may be explained by the negative sugar moiety having sufficient regions to interact with the protein at low charge states when well folded and compact, but as unfolding is induced by charge addition the sugar molecules have fewer favourable interactions with the protein and add to the cross-section as they project away from the backbone into space.

Between $z = 17^+$ and 20^+, all four species exhibit a possible unfolding event as the cross-sections increase at a greater rate than elsewhere (425, 601, 694 and 1086 Å^2 for two, three, four and five bound GlcNAc fH 10–15 respectively). The largest of these increases, for the five bound sugar fH 10–15 molecule, may indicate that a number of the covalently bound sugars are no longer interacting closely with the protein as these non-specific binding sites have been lost through protein unfolding, with bond angles and distances for favourable interactions now out of range.

Synapt fH 10–15 values are more compact at low charge states and more extended at high charge states than for MoQTOF data. This contrasts with the data obtained for p53 and for fH 19–20. In comparing Synapt and MoQTOF mass spectra of fH 10–15, the data taken on the Synapt shows a charge state distribution that is centered at higher charge values (22^+) than that on the MoQToF (14^+) (Fig. 4). As solution conditions were identical for these two spectra the slight differences in the charge state distributions and the collision cross-sections must be due to the differences in desolvation on transfer to the gas phase resulting in conformational changes. As desolvation occurs any denatured protein present collapses and electrostatic interactions, rather than hydrophilic, dominate the final geometry adopted. This may be the case for the formation of more compact geometries at the low charge states of fH 10–15 (Synapt data), as the less constrained denatured protein geometries in solution collapse in the gas phase.

3.7. fH 19–20 mass spectrometry

3.7.1. Synapt

fH 19–20 (M_R = 14,743.8 Da) was sprayed from 20 mM ammonium acetate buffer solution containing 10% propan-2-ol by volume at a wave height of 8 V. Four charge states were observed from $z = 7^+$ to 10^+ with the 8^+ charge state dominant as shown in Fig. 5A. This narrow charge state distribution and relatively low charge indicates a native-like solution-phase structure transferred to the gas phase. During the protein expression method, two additional residues (E and A) have been covalently incorporated into the protein population as a recombinant impurity. This is observed as a peak at higher *m/z* for all four charge states.

3.7.2. MoQTOF

fH 19–20 was sprayed from the same solvent conditions as above producing five monomer charge states ($z = 6^+$ to 10^+; 9^+ dominant) as shown in Fig. 5B. The relatively narrow charge state distribution centered on the most abundant peak, $z = 9^+$, again indicates an overall folded protein structure. Upon interrogating the mass spectrum above 2000 *m/z*, a plethora of dimeric species can be elucidated. Due to a recombinant impurity of the two residues (EA), three possible dimer species may be produced: a dimer with both monomers not containing the recombinant impurity; a dimer with one monomer subunit having no impurity and one monomer containing the impurity; and a dimer with both monomers containing the impurity. All three of dimer species are displayed for $z = 13^+$ (2269.3, 2284.7 and 2300.0 *m/z* respectively). From the intensity of the surrounding dimer peaks, we have assigned with confidence, dimer peaks with $z = 11^+$ to 14^+. Evenly charged dimer *m/z* values are concomitant with those of a monomer with half the charge, so care has been taken when assigning monomers with $z = 6^+$ and 7^+ and their respective dimers with $z = 12^+$ and 14^+.

Both instruments successfully transfer native-like fH 19–20 into the gas phase as shown by the narrow charge state distributions. Protein with and without the recombinant error are clearly observed on all peaks. MoQTOF data show considerably more gas-phase species which include all three forms of the dimer as well as poorly resolved higher *m/z* species such as the 5^+ monomer.

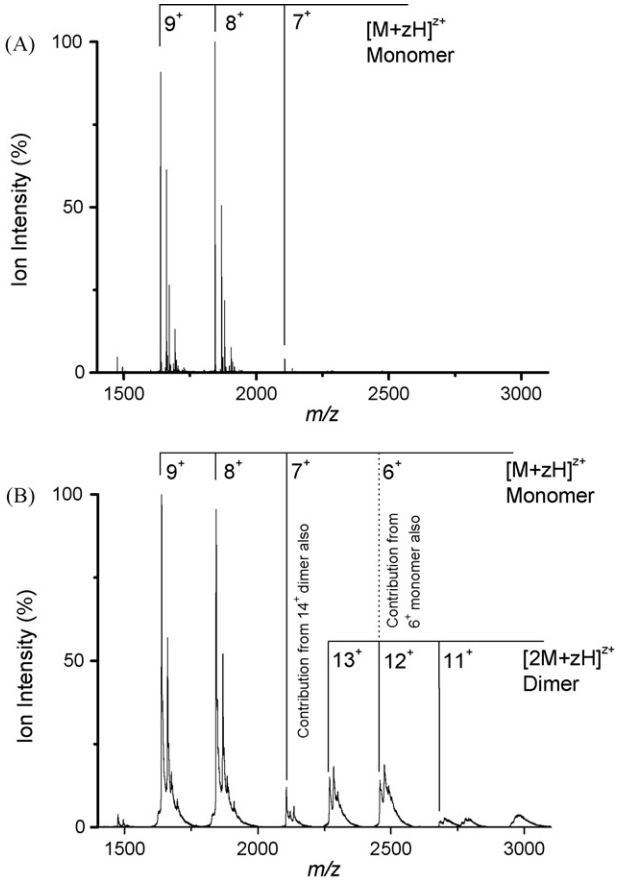

Fig. 5. Mass spectra of native-like fH 19–20 sprayed from 20 mM ammonium acetate and 10% propan-2-ol on the Synapt (A) and the MoQTOF (B).

3.8. fH 19–20 ion mobility-mass spectrometry

3.8.1. Synapt

Collision cross-sections for four charge states ($z = 7^+$ to 10^+) of fH 19–20 were calculated with a single conformer characterised for $z = 7^+$ and 10^+, and two conformers characterised for $z = 8^+$ and 9^+ as shown in Table 5. Cross-section increases near-linearly with charge as can be seen from Fig. 6 (closed squares) with an overall increase from 7^+ to 10^+ of 21.8% indicative of an initially well structured protein undergoing minor structural rearrangement. The two conformers of the 8^+ and 9^+ charge states are of similar collision cross-section (1729 and 1743 Å^2 respectively) and may have adopted similar gas-phase structures.

Table 5
Collision cross-sections of Factor H 19–20 obtained from Synapt (8 V wave height) and MoQTOF data.

Charge state (z^+)	Collision cross-section (Å^2) on Synapt	Collision cross-section (Å^2) on MoQTOF
6	–	1227
		1343
7	1328	1214
	–	1295
8	1443	1328
	1729	1479
9	1556	1364
	1743	1545
10	1699	1667
	–	1904

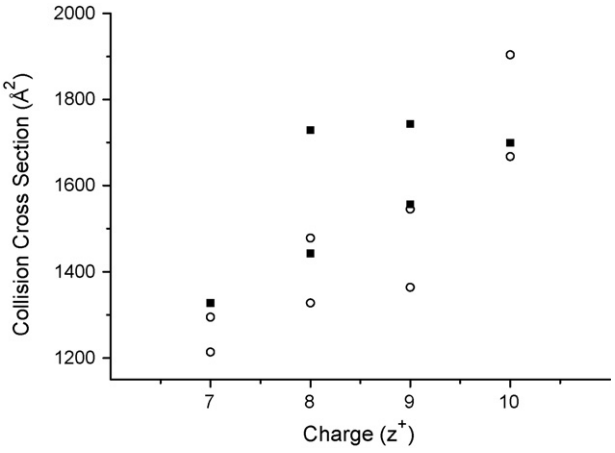

Fig. 6. Collision cross-sections versus z for $[M+zH]^{z+}$ where M = fH 19–20. Synapt data is shown by closed squares and MoQTOF by open circles.

3.8.2. MoQTOF

Collision cross-sections for five monomer charge states, $z = 6^+$ to 10^+, and four dimer charge states, $z = 11^+$ to 14^+, could be elucidated using the MoQTOF instrument (Tables 5 and 6). Two conformers for all monomer and dimer charge states were elucidated. Monomer cross-sections ranged from 1227 Å^2 for the smallest conformer of $z = 6^+$ to 1904 Å^2 for the largest conformer with $z = 10^+$. Fig. 6 is a comparison plot between MoQTOF and Synapt data for the monomer charge states.

Again, cross-section values obtained from the MoQTOF are smaller than obtained from the Synapt but here there is a much greater agreement in values. Cross-sections for $z = 7^+$ to 10^+ for Synapt and MoQTOF are between 0.7% and 2.5% for one conformer at each of these charge states.

As discussed in the fH 19–20 mass spectrometry section, three dimeric species were observed. For $z = 11^+$, only the impurity-free dimer (*i.e.*, both monomer subunits do not have additional glutamic acid or alanine residues present) was interrogated producing cross-sections of 1933 and 2240 Å^2 as further dimer species could not be resolved. For $z = 12^+$ and 14^+, the dimer containing one impurity monomer could be unambiguously identified (2475.0 and 2121.5 m/z for $z = 12^+$ and 14^+ respectively) in the ion mobility-mass spectrum and two conformers for each charge state were elucidated.

Using Origin 7.5 curve fitting software, Gaussian peaks were fitted to the arrival time distributions of each drift voltage (within a charge state) to extract overlapping dimer and monomer information. This method, along with observing the peak intensity in the mass spectrum, allowed us to elucidate cross-sections for the evenly charged monomer and dimer species.

Finally, the $z = 13^+$ charge state provided full elucidation of all three dimeric species as the m/z values did not interfere with any other species. Protein dimer free from impurities has the most compact geometry of the three dimeric species, with one conformer having a cross-section (2449 Å^2) similar to the addition of the two smaller monomer conformers of 6^+ and 7^+ (2441 Å^2). The other dimer conformer (2279 Å^2) cross-section is smaller than mere addition of two monomer subunits and may provide evidence for folding and structural arrangement. The overall change in cross-section upon incorporating one or two monomer subunits with the recombinant impurity is not more than 4.4%—a small contribution to cross-section as would be expected for addition of only two residues to a protein chain.

Cross-sections were calculated for four charge states using Synapt data, with two of these charge states having a single conformer, and the other two having two conformers. No dimer cross-sections could be produced at wave height at 8 V, however

Table 6
Collision cross-sections of Factor H 19–20 dimer species obtained from MoQTOF data.

Charge state (z^+)	Protein dimer impurity absent (M_R = 14,743.8 Da)	Protein dimer 1 monomer with EA impurity (M_R = 14,943.8 Da)	Protein dimer both monomers with EA impurity (M_R = 29,887.6 Da)
11	1933 2240	–	–
12	–	2198 2442	–
13	2279 2449	2314 2562	2304 2457
14	–	2414 2606	–

using a variable wave height gradient of 8–10 V allowed the observation of a small dimer species with $z = 13^+$ which presented only a single conformer. We have not calculated the collision cross-section for this species. MoQTOF data allowed a larger number of gas-phase species to be analysed and cross-sections elucidated for five monomer charge states with two conformations for each. Additionally, three dimeric species could be characterised for the $z = 13^+$ dimer species. Dimer containing no EA impurity could be characterised for the $z = 11^+$ charge state and dimers with one monomer subunit containing EA were characterised for $z = 12^+$ and 14^+.

3.9. Factor H 19–20 comparison to condensed-phase data

Published structures are available from the Research Collaboratory for Structural Bioinformatics (RCSB) [53] for module fH 19–20: NMR structure (PDB ID: 2BZM [48]) and XRC structure (PDB ID: 2G7I [54]). Using MOBCAL, three computational methods (1, projection approximation method; 2, trajectory method; 3, exact hard-sphere scattering method) [19] can provide theoretical collision cross-sections from coordinates obtainable from NMR structures or XRC atomic coordinates which can then be compared to experimental data. We will not present projection approximation cross-sections for systems of this size as this method ignores the effect of multiple collisions of a given drift gas atom with the molecular ion, which for molecules of >200 atoms, yields collision cross-sections that are progressively too small and therefore are greatly misleading, particularly for large systems such as fH 19–20.

For the 10 deposited NMR structures of fH 19–20, an average theoretical collision cross-section of 1923 Å^2 was obtained using the exact hard-sphere scattering (EHSS) method where the ion is modelled by a collection of overlapping hard spheres with radii equal to hard sphere collision distances. The orientationally averaged momentum transfer cross-section is calculated by determining the scattering angles between the incoming buffer gas atom trajectory and the departing buffer gas atom trajectory. Using the same NMR structures, the full trajectory method (TM) yields an average collision cross-section of 1907 Å^2 with a range of cross-sections from 1850 to 1942 Å^2. These values are in good agreement with one of the $z = 10^+$ monomer conformers (1904 Å^2) as would be expected for a native-like protein when compared with solution-phase data. However the lower charge states exhibit significantly lower collision cross-sections than this. Native protein transfer from solution to gas phase is likely to result in gas-phase collapse due to desolvation, causing residue side chains that were solvated to collapse back against the protein, and generally the absence of stabilising buffer salts and the increased contribution of electrostatic interactions may have the effect of 'shrinking' the protein. We have previously reported on this phenomena [29]. Such a collapse of tertiary structure from this protein, which is dominated by loose β-sheets, is to be expected and is supported by the lower cross-sections of lower charge states.

4. Conclusions

Two different ion mobility instruments have been used to study the gas-phase collision cross-sections of three biologically relevant protein systems which had not yet been studied using this technique. Comparison between mass spectra and cross-section results for each of these protein molecules have provided initial insights into the stability of protein structures on transfer into the gas phase and also the contribution of coulombically driven unfolding.

p53 protein was sprayed under native-like conditions on Synapt HDMS and MoQTOF instruments. Mass spectra charge state distributions were in good agreement, with base peaks at $z = 9^+$ and 10^+ respectively. Multimeric species (dimers) were observed in both instruments in the presence of zinc which may have some biological relevance as the active form of the full-length protein is postulated to be a dimer of dimers [55,56]. No dimer was observable in the absence of zinc. Subjecting the protein to ion mobility separation yielded conformations for each charge state with collision cross-sections indicating a protein unfolding event in the charge state range $z = 11^+$ to 15^+. Cross-section values obtained on the MoQTOF instrument were at times smaller (more compact) than those found on the Synapt, which may be attributable to slight solution differences as well as to the differences in the source transfer regions of the two instruments affecting gas-phase conformations.

Phenanthroline dissolved in ammonium acetate buffer was used as a chelating agent to remove a potentially important zinc ion from p53. The protein was analysed on both instruments and cross-sections again measured. Synapt values indicate a Coulombic repulsion-driven unfolding over the entire charge state measured ($z = 9^+$ to 15^+) whereas MoQTOF data, in line with better preserving native interactions, displays compact conformers at low charge state leading to an unfolding event at higher charge (between $z = 11^+$ and 13^+). MoQTOF values are again smaller overall compared to Synapt.

Factor H is a large glycoprotein composed of a "string of beads" formation of twenty complement modules. Two regions of the protein, 10–15 and 19–20 were analysed by MS and IM-MS on both instruments for comparison and structure characterisation. fH 10–15 mass spectra differed with Synapt data's base peak at $z = 22^+$ compared with $z = 14^+$ on the MoQTOF. Current evidence suggests, at least for globular soluble proteins, good native nano-electrospray ionisation conditions will give rise to narrow charge state distributions with a base peak at relatively low charge states [57], indicating a more denatured protein on the Synapt. The expression system gave rise to three to six molecules of N-acetylglucosamine sugar bound to the protein module. These sugar molecules did not significantly affect the protein cross-section due to their size (220 Da) compared to the protein size (~41 kDa). MoQTOF mass spectra displayed the same covalent artefacts however here two to five molecules of the sugar were resolvable. Again the addition of sequential covalent modifications did not affect the collision

cross-sections of the protein. Finally, the C-terminal region of Factor H (19–20) was investigated. Mass spectrometry data from the Synapt provided evidence for a native-like protein with a narrow charge state of low charge (base peak $z = 8^+$). MoQTOF data provided the same charge state distribution, but with contributions from gas-phase dimer species which were resolved using enhanced Gaussian fittings to arrival time distributions. A recombinant artefact in the protein expression method produced a population of protein molecules with an additional two amino acid residues (alanine and glutamic acid) which could be clearly observed in the mass spectrum. These additional peaks proved useful in characterising monomer and dimer contributions at concomitant m/z values. Cross-sections for monomer subunits were in good agreement (less than 2.5%) between Synapt and MoQTOF data, and all conformers (bar the larger $z = 10^+$ conformer) were more compact than the computationally derived cross-section from the NMR structure. Dimers were not observed on the Synapt instrument, however up to three dimer species were seen on the MoQTOF for which cross-sections could be extracted.

The data presented in this paper on three biologically relevant systems shows that different sources can produce molecular ions with somewhat different collision cross-sections even from the same starting solution conditions. This is also evident in the different charge state distributions that can be obtained in the acquired mass spectra. Multimeric gas-phase species (predominantly dimers) were more abundant in our MoQTOF studies. Mass spectra from the MoQTOF indicate that in our hands the source is providing more 'native-like' conformations since the charge state distributions centre on lower charge states. This may be attributed to enhanced control of source pressure and mobility being measured in an environment where the temperature of the buffer gas is carefully measured and included in the calculation of mobility. We had limited time on the Synapt instrument and cannot rule out the possibility of obtaining closer collision cross-sections from the systems examined given more time. The data also shows that coulombically driven unfolding of proteins is both system and source dependent, and can vary with respect to charge. Much more experimental comparison of collision cross-sections obtained for native nano-electrosprayed proteins on Synapt and drift tube ion mobility instrumentation, coupled with reference to solution and/or crystal structures, will further validate and support the use of ion mobility-mass spectrometry as a tool for structural biology on large and multimeric protein assemblies.

Acknowledgements

This research was supported by the EPSRC grants GR/S77639/01 and EP/C541561/1 and in particular *via* the award of an Advanced Research Fellowship to PEB and a studentship in conjunction with the RSC Analytical Trust Fund to PAF. All of the Synapt work was undertaken at the Waters MS Technologies Centre Manchester. We also had support from the BBSRC, the Royal Society, the British Mass Spectrometry Society, and Waters Corporation Manchester and in particular we thank Steven Pringle, Kevin Giles, Jason Wildgoose and Robert Bateman. We also are grateful for continuing support from the School of Chemistry at the University of Edinburgh.

Appendix A. Supplementary data

Supplementary data associated with this article can be found, in the online version, at doi:10.1016/j.ijms.2010.01.007.

References

[1] E. van Duijn, P.J. Bakkes, R.M. Heeren, R.H. van den Heuvel, H. van Heerikhuizen, S.M. van der Vies, A.J. Heck, Monitoring macromolecular complexes involved in the chaperonin-assisted protein folding cycle by mass spectrometry, Nat. Methods 2 (5) (2005) 371–376.
[2] F. Sobott, M.G. McCammon, H. Hernandez, C.V. Robinson, The flight of macromolecular complexes in a mass spectrometer, Philos. Transact. A Math Phys. Eng. Sci. 363 (1827) (2005) 379–389 (discussion 389-91).
[3] J.L.P. Benesch, B.T. Ruotolo, D.A. Simmons, C.V. Robinson, Protein complexes in the gas phase: technology for structural genomics and proteomics, Chem. Rev. 107 (8) (2007) 3544–3567.
[4] B.T. Ruotolo, C.V. Robinson, Aspects of native proteins are retained in vacuum, Curr. Opin. Chem. Biol. 10 (5) (2006) 402–408.
[5] J.L.P. Benesch, C.V. Robinson, Mass spectrometry of macromolecular assemblies: preservation and dissociation, Curr. Opin. Struct. Biol. 16 (2) (2006) 245–251.
[6] A.A. Rostom, P. Fucini, D.R. Benjamin, R. Juenemann, K.H. Nierhaus, F.U. Hartl, C.M. Dobson, C.V. Robinson, Detection and selective dissociation of intact ribosomes in a mass spectrometer, Proc. Natl. Acad. Sci. U.S.A. 97 (10) (2000) 5185–5190.
[7] B.C. Bohrer, S.I. Merenbloom, S.L. Koeniger, A.E. Hilderbrand, D.E. Clemmer, Biomolecule analysis by ion mobility spectrometry, Annu. Rev. Anal. Chem. 1 (1) (2008) 293–327.
[8] D.E. Clemmer, M.F. Jarrold, Ion mobility measurements and their applications to clusters and biomolecules, J. Mass Spectrom. 32 (6) (1997) 577–592.
[9] C.A. Scarff, K. Thalassinos, G.R. Hilton, J.H. Scrivens, Travelling wave ion mobility mass spectrometry studies of protein structure: biological significance and comparison with X-ray crystallography and nuclear magnetic resonance spectroscopy measurements, Rapid Commun. Mass Spectrom. 22 (20) (2008) 3297–3304.
[10] C. Becker, F.A. Fernandez-Lima, K.J. Gillig, W.K. Russell, S.M. Cologna, D.H. Russell, A novel approach to collision-induced dissociation (CID) for ion mobility-mass spectrometry experiments, J. Am. Soc. Mass Spectrom. 20 (6) (2009) 907–914.
[11] L. Jin, P.E. Barran, J.A. Deakin, M. Lyon, D. Uhrin, Conformation of glycosaminoglycans by ion mobility mass spectrometry and molecular modelling, Phys. Chem. Chem. Phys. 7 (19) (2005) 3464–3471.
[12] E.R. Badman, C.S. Hoaglund-Hyzer, D.E. Clemmer, Dissociation of different conformations of ubiquitin ions, J. Am. Soc. Mass Spectrom. 13 (6) (2002) 719–723.
[13] D.E. Clemmer, R.R. Hudgins, M.F. Jarrold, Naked protein conformations: cytochrome *c* in the gas phase, J. Am. Chem. Soc. 117 (40) (1995) 10141–10142.
[14] R.T. Kurulugama, S.J. Valentine, R.A. Sowell, D.E. Clemmer, Development of a high-throughput IMS-IMS-MS approach for analyzing mixtures of biomolecules, J. Proteomics 71 (3) (2008) 318–331.
[15] S.J. Valentine, M.D. Plasencia, X. Liu, M. Krishnan, S. Naylor, H.R. Udseth, R.D. Smith, D.E. Clemmer, Toward plasma proteome profiling with ion mobility-mass spectrometry, J. Proteome Res. 5 (11) (2006) 2977–2984.
[16] S.I. Merenbloom, S.L. Koeniger, B.C. Bohrer, S.J. Valentine, D.E. Clemmer, Improving the efficiency of IMS-IMS by a combing technique, Anal. Chem. 80 (6) (2008) 1918–1927.
[17] B.T. Ruotolo, S.J. Hyung, P.M. Robinson, K. Giles, R.H. Bateman, C.V. Robinson, Ion mobility-mass spectrometry reveals long-lived, unfolded intermediates in the dissociation of protein complexes, Angew. Chem. Int. Ed. Engl. 46 (42) (2007) 8001–8004.
[18] E.R. Badman, S. Myung, D.E. Clemmer, Evidence for unfolding and refolding of gas-phase cytochrome *c* ions in a Paul trap, J. Am. Soc. Mass Spectrom. 16 (9) (2005) 1493–1497.
[19] A.A. Shvartsburg, M.F. Jarrold, An exact hard-spheres scattering model for the mobilities of polyatomic ions, Chem. Phys. Lett. 261 (1–2) (1996) 86–91.
[20] M.F. Mesleh, J.M. Hunter, A.A. Shvartsburg, G.C. Schatz, M.F. Jarrold, Structural information from ion mobility measurements: effects of the long-range potential, J. Phys. Chem. 100 (40) (1996) 16082–16086.
[21] E. Murray, D.J. Clarke, H.V. Florance, C.L. MacKay, P. Langridge-Smith, T.R. Hupp, Proteasomal-dependent degradation of anterior gradient-2 is regulated by an oxidant-responsive dimerisation, submitted for publication.
[22] K. Giles, S.D. Pringle, K.R. Worthington, D. Little, J.L. Wildgoose, R.H. Bateman, Applications of a travelling wave-based radio-frequency-only stacked ring ion guide, Rapid Commun. Mass Spectrom. 18 (20) (2004) 2401–2414.
[23] S.D. Pringle, K. Giles, J.L. Wildgoose, J.P. Williams, S.E. Slade, K. Thalassinos, R.H. Bateman, M.T. Bowers, J.H. Scrivens, An investigation of the mobility separation of some peptide and protein ions using a new hybrid quadrupole/travelling wave IMS/oa-ToF instrument, Int. J. Mass Spectrom. 261 (1) (2007) 1–12.
[24] T. Wyttenbach, P.R. Kemper, M.T. Bowers, Design of a new electrospray ion mobility mass spectrometer, Int. J. Mass Spectrom. 212 (1–3) (2001) 13–23.
[25] C.S. Creaser, J.R. Griffiths, C.J. Bramwell, S. Noreen, C.A. Hill, C.L.P. Thomas, Ion mobility spectrometry: a review. Part 1. Structural analysis by mobility measurement, Analyst 129 (11) (2004) 984–994.
[26] D. Wittmer, Y.H. Chen, B.K. Luckenbill, H.H. Hill, Electrospray ionization ion mobility spectrometry, Anal. Chem. 66 (14) (1994) 2348–2355.
[27] E.A. Mason, E.W. McDaniel, Transport Properties of Ions in Gases, Wiley, New York, 1988.
[28] B.J. McCullough, J. Kalapothakis, H. Eastwood, P. Kemper, D. MacMillan, K. Taylor, J. Dorin, P.E. Barran, Development of an ion mobility quadrupole time of flight mass spectrometer, Anal. Chem. 80 (16) (2008) 6336–6344.
[29] P.A. Faull, K.E. Korkeila, J.M. Kalapothakis, A. Gray, B.J. McCullough, P.E. Barran, Gas-phase metalloprotein complexes interrogated by ion mobility-mass spectrometry, Int. J. Mass Spectrom. 283 (1-3) (2009) 140–148.

[30] K.H. Vousden, D.P. Lane, p53 in health and disease, Nat. Rev. Mol. Cell Biol. 8 (4) (2007) 275–283.
[31] D.P. Lane, p53, guardian of the genome, Nature 358 (6381) (1992) 15–16.
[32] S.A. Showalter, L. Bruschweiler-Li, E. Johnson, F. Zhang, R. Bruschweiler, Quantitative lid dynamics of MDM2 reveals differential ligand binding modes of the p53-binding cleft, J. Am. Chem. Soc. 130 (20) (2008) 6472–6478.
[33] A. Dey, V. Tergaonkar, D.P. Lane, Double-edged swords as cancer therapeutics: simultaneously targeting p53 and NF-[kappa]B pathways, Nat. Rev. Drug Discov. 7 (12) (2008) 1031–1040.
[34] D. Alarcon-Vargas, Z. Ronai, p53-Mdm2—the affair that never ends, Carcinogenesis 23 (4) (2002) 541–547.
[35] S.L. Harris, A.J. Levine, The p53 pathway: positive and negative feedback loops, Oncogene 24 (17) (2005) 2899–2908.
[36] P.H. Kussie, S. Gorina, V. Marechal, B. Elenbaas, J. Moreau, A.J. Levine, N.P. Pavletich, Structure of the MDM2 oncoprotein bound to the p53 tumor suppressor transactivation domain, Science 274 (5289) (1996) 948–953.
[37] P. Hainaut, K. Mann, Zinc binding and redox control of p53 structure and function, Antioxid. Redox Signal. 3 (4) (2001) 611–623.
[38] C. Meplan, M.J. Richard, P. Hainaut, Metalloregulation of the tumor suppressor protein p53: zinc mediates the renaturation of p53 after exposure to metal chelators in vitro and in intact cells, Oncogene 19 (46) (2000) 5227–5236.
[39] M. Reed, Y. Wang, G. Mayr, M.E. Anderson, J.F. Schwedes, P. Tegtmeyer, p53 domains: suppression, transformation, and transactivation, Gene Expr. 3 (1) (1993) 95–107.
[40] Y. Wang, M. Reed, P. Wang, J.E. Stenger, G. Mayr, M.E. Anderson, J.F. Schwedes, P. Tegtmeyer, p53 domains: identification and characterization of two autonomous DNA-binding regions, Genes Dev. 7 (12B) (1993) 2575–2586.
[41] J.M.P. Canadillas, H. Tidow, S.M.V. Freund, T.J. Rutherford, H.C. Ang, A.R. Fersht, Solution structure of p53 core domain: structural basis for its instability, Proc. Natl. Acad. Sci. U.S.A. 103 (7) (2006) 2109–2114.
[42] M. Olivier, R. Eeles, M. Hollstein, M.A. Khan, C.C. Harris, P. Hainaut, The IARC TP53 database: new online mutation analysis and recommendations to users, Hum. Mutat. 19 (6) (2002) 607–614.
[43] M.J. Walport, Complement. Second of two parts, N. Engl. J. Med. 344 (15) (2001) 1140–1144.
[44] M.J. Walport, Complement. First of two parts, N. Engl. J. Med. 344 (14) (2001) 1058–1066.
[45] C.Q. Schmidt, A.P. Herbert, D. Kavanagh, C. Gandy, C.J. Fenton, B.S. Blaum, M. Lyon, D. Uhrin, P.N. Barlow, A new map of glycosaminoglycan and C3b binding sites on factor H, J. Immunol. 181 (4) (2008) 2610–2619.
[46] M.R. Buddles, R.L. Donne, A. Richards, J. Goodship, T.H. Goodship, Complement factor H gene mutation associated with autosomal recessive atypical hemolytic uremic syndrome, Am. J. Hum. Genet. 66 (5) (2000) 1721–1722.
[47] G.S. Hageman, D.H. Anderson, L.V. Johnson, L.S. Hancox, A.J. Taiber, L.I. Hardisty, J.L. Hageman, H.A. Stockman, J.D. Borchardt, K.M. Gehrs, R.J. Smith, G. Silvestri, S.R. Russell, C.C. Klaver, I. Barbazetto, S. Chang, L.A. Yannuzzi, G.R. Barile, J.C. Merriam, R.T. Smith, A.K. Olsh, J. Bergeron, J. Zernant, J.E. Merriam, B. Gold, M. Dean, R. Allikmets, A common haplotype in the complement regulatory gene factor H (HF1/CFH) predisposes individuals to age-related macular degeneration, Proc. Natl. Acad. Sci. U.S.A. 102 (20) (2005) 7227–7232.
[48] A.P. Herbert, D. Uhrin, M. Lyon, M.K. Pangburn, P.N. Barlow, Disease-associated sequence variations congregate in a polyanion recognition patch on human Factor h revealed in three-dimensional structure, J. Biol. Chem. 281 (24) (2006) 16512–16520.
[49] B.T. Ruotolo, J.L. Benesch, A.M. Sandercock, S.J. Hyung, C.V. Robinson, Ion mobility-mass spectrometry analysis of large protein complexes, Nat. Protoc. 3 (7) (2008) 1139–1152.
[50] P.V. Nikolova, K.B. Wong, B. DeDecker, J. Henckel, A.R. Fersht, Mechanism of rescue of common p53 cancer mutations by second-site suppressor mutations, Embo. J. 19 (3) (2000) 370–378.
[51] S. Patel, T.T.T. Bui, A.F. Drake, F. Fraternali, P.V. Nikolova, The p73 DNA binding domain displays enhanced stability relative to its homologue, the tumor suppressor p53, and exhibits cooperative DNA binding, Biochemistry 47 (10) (2008) 3235–3244.
[52] S. Patel, R. George, F. Autore, F. Fraternali, J.E. Ladbury, P.V. Nikolova, Molecular interactions of ASPP1 and ASPP2 with the p53 protein family and the apoptotic promoters PUMA and Bax, Nucl. Acids Res. 36 (16) (2008) 5139–5151.
[53] H.M. Berman, J. Westbrook, Z. Feng, G. Gilliland, T.N. Bhat, H. Weissig, I.N. Shindyalov, P.E. Bourne, The protein data bank, Nucl. Acids Res. 28 (1) (2000) 235–242.
[54] T.S. Jokiranta, V.P. Jaakola, M.J. Lehtinen, M. Parepalo, S. Meri, A. Goldman, Structure of complement factor H carboxyl-terminus reveals molecular basis of atypical haemolytic uremic syndrome, Embo. J. 25 (8) (2006) 1784–1794.
[55] W.C. Ho, M.X. Fitzgerald, R. Marmorstein, Structure of the p53 core domain dimer bound to DNA, J. Biol. Chem. 281 (29) (2006) 20494–20502.
[56] K.G. McLure, P.W. Lee, How p53 binds DNA as a tetramer, Embo J. 17 (12) (1998) 3342–3350.
[57] R.H.H. van den Heuvel, A.J.R. Heck, Native protein mass spectrometry: from intact oligomers to functional machineries, Curr. Opin. Chem. Biol. 8 (5) (2004) 519–526.